arXiv:1911.06688v2 [cond-mat.stat-mech] 24 Jan 2020

How a local active force modifies the structural properties of polymers

L. Natali[1], L. Caprini[1], and F. Cecconi[3]
1, *Dipartimento di Fisica, Università "Sapienza", Piazzale A. Moro 5, I00185 Rome Italy.*
[2] *Gran Sasso Science Institute (GSSI), Via. F. Crispi 7, 67100 L'Aquila, Italy. E-mail: lorenzo.caprini@gssi.it*
[3], *Istituto dei Sistemi Complessi-CNR, Via Taurini 19, I-00185 Rome Italy.*
(Dated: February 7, 2022)

We study the dynamics of a polymer, described as a variant of a Rouse chain, driven by an active terminal monomer (head). The local active force induces a transition from a globule-like to an elongated state, as revealed by the study of the end-to-end distance, whose variance is analytically predicted under suitable approximations. The change in the relaxation times of the Rouse-modes produced by the local self-propulsion is consistent with the transition from globule to elongated conformations. Moreover also the bond-bond spatial correlation for the chain head results to be affected and a gradient of over-stretched bonds along the chain is observed. We compare our numerical results both with the phenomenological stiff-polymer theory and several analytical predictions in the Rouse-chain approximation.

I. INTRODUCTION

Active matter includes a large class of physical and biological entities ranging from microscopic to macroscopic length scales. Active systems usually convert fuel energy from the environment into directed motion using chemical reactions [1] or propelling in a fluid through flagella, cilia or more complex mechanisms [2]. Although numerous studies have focused on spherical rigid or rod-like microswimmers, many active systems, appears in polymeric and filamentous structures which often undergo stretching or deformations. In particular, the cell cytoskeleton contains many active filaments, like actins and microtubules [3, 4]. Recently, microtubules have been studied in vitro and transported along a glass substrate by ATP fueled motor proteins [5].

Out of the biological realm, it is even possible to realize synthetic active colloidal polymers [6], such as chains of colloids uniformly coated with catalytic particles [7] becoming active when immersed in a solution of H_2O_2. The "activation" of Janus particles can be even controlled by external fields, and, in particular, the spontaneous formation of chains of particles has been experimentally observed upon tuning the frequencies of an AC electric field [8–10].

The study of active or activated flexible and semiflexible polymers has received much attention in the last years, for both biological interest and possible applications towards the design of new materials with peculiar properties. Several authors, via computer simulations, addressed not only the "activation" of polymers [11–13] but also studied the behavior of polymer chains immersed into an active bath [14–19]. Sometimes, the activation is modeled by imposing a self-propulsion force tangential to the filament [20–24], while the common approach for the effect of an active bath amounts to considering the monomer under independent active forces [12, 13, 16, 25]. In any case, the interplay between active forces and extended flexible structures gives rise to a rich phenomenology also including collective behaviors [26–32]. For instance, a freely moving active filament takes on peculiar dynamical conformations performing: rotational, straight translational [33, 34], snake-like [21, 22] and even helical motion [35]. In addition, in the limit of large active forces, both semi-flexible and flexible polymers swell [12, 13] while clamped filaments exhibit beating and rotational motion under tangential forces [23, 36, 37]. In some cases, compactification and shrinkage of structures occur at very strong active forces [38, 39], and at high densities swirls and spirals are induced by the increase of the active force [31]. Some authors implemented the activity, generated by the release of energy due to ATP hydrolysis, as a temperature increase observing phase-separations in binary mixture of passive-active polymers [40, 41].

The studies mentioned above deal with global activated polymers. However, there are biological examples in which the self-propulsion is generated only in local regions of the active particle. For instance, some elongated bacteria move thanks to cilia attached to specific regions of their body, analogously, spermatozoa swim due to single flagellum protruding from the body. Other examples come from the action of RNA polymerase on DNA or kinesin on microtubules, which are generally described as molecular motors on polymer substrates [42]. Thus, for long and flexible swimmers, we need to go beyond the collective activation or center of mass description, because the interplay between deformability and self-propulsion induces a richer phenomenology.

Some authors considered polymers with a catalytic terminal (head)[43, 44], where the chemical reactions occurring at the head produce a local self-propulsion which increases the effective diffusivity of the chain.

Motivated by these works, we study the activation of the terminal monomer of a polymer, modeling the self-propulsion in the framework of non-equilibrium stochastic processes. In particular, we adopt a well-established model, known as Active Ornstein-Uhlenbeck (AOUP) model [45–50] to describe the self-propulsion at a coarse-grained level, neglecting the microscopic details of the

active force. We describe the behavior of the polymer in the absence of any confinement or external potential to determine how a local active force affects the chain conformations.

This paper is organized as follows. In Sec. II, we introduce the model describing the polymer in the presence of a local active force, activated only on the last monomer, while, in Sec. III, we present numerical results in the absence of any external mechanism or molecular motor. We focus, on one hand, on the study of the end-to-end distance and, on the other hand, on the structural microscopic properties of the polymer, unveiling the effect of the local active force. Finally, we summarize the results and discuss some future perspectives in the conclusive Section.

II. A FREE POLYMER WITH AN ACTIVE HEAD

To model a polymeric structure, such as proteins or biological filaments, we employ a variant of the Rouse-chain [51], assuming that each monomer has the same structure and composition. Each monomer is only connected to the nearest neighbors by springs of strength k and rest length $\sigma > 0$. Since we neglect the steric interactions among non-consecutive beads the polymer is fully described by the simple potential:

$$U(\mathbf{r}_1, \ldots, \mathbf{r}_N) = \frac{k}{2} \sum_{n=1}^{N-1} (|\mathbf{r}_{n+1} - \mathbf{r}_n| - \sigma)^2 \tag{1}$$

and its dynamics is ruled by N coupled Langevin equations for the positions and velocities of each monomer, $\mathbf{r}_n$, and $\mathbf{v}_n$, respectively:

$$\dot{\mathbf{x}}_n = \mathbf{v}_n \tag{2a}$$

$$\dot{\mathbf{v}}_n = -\frac{\mathbf{v}_n}{\tau_0} - \frac{\partial U}{\partial \mathbf{r}_n} + \frac{\sqrt{2D_t}}{\tau_0}\boldsymbol{\xi}_n + \delta_{n,N}\mathbf{f}_a\,, \tag{2b}$$

where τ_0 is the inertial relaxation time of each monomer. $\boldsymbol{\xi}_n$ is a white noise vector whose uncorrelated components have zero averages and unit variances, while D_t is the diffusion coefficient due to the solvent. The last term, $\delta_{n,N}\mathbf{f}_a$, represents the active force, due, for instance, to ATP-hydrolysis or other chemical reactions occurring at a catalytic site. Since we assume that the reaction takes place on one terminal only, we denote such a monomer as "catalytic head".

To describe the fluctuations of the active force, we employ the Ornstein-Uhlenbeck process (AOUP model)

$$\tau\dot{\mathbf{f}}_a = -\mathbf{f}_a + \sqrt{2D_a}\boldsymbol{\eta}\,, \tag{3}$$

being $\boldsymbol{\eta}$ a white noise vector with zero averages and unit variances. The two-time activity-activity correlation of $\mathbf{f}_a$ decays exponentially, with a correlation time, τ, that roughly determines the time-window after which the active force completely resets its value. We remark that the AOUP model constitutes a simplification of the Active Brownian Particle model (ABP) [52–55] which is known to explain the well-known phenomenology of spherical self-propelled particles [46, 56–59]. The connection between AOUP and ABP has been shown by several authors [60, 61]. In Eq.(3), the parameter $\sqrt{D_a/\tau}$ has a particular relevance because it sets the strength of the self-propulsion. In other terms, a single particle performs a persistent motion in the direction of $\mathbf{f}_a$ for a time $t < \tau$, while for $t > \tau$ a diffusive-like behavior of a passive Brownian particle with a certain effective temperature is recovered. When τ is the smallest time scale in the system, the active force can be simply recast into a Brownian motion $\mathbf{f}_a \approx \sqrt{2D_a}\boldsymbol{\eta}$, being $\mathbf{f}_a$ the faster degree of freedom whose time-derivative could be set to zero. We expect that in such a case the head does not display any persistence and the role of the active force leads just to the increase of the effective diffusion. In addition, in order to enhance the effect of the self-propulsion, we focus on a regime where the velocity of the monomers relaxes faster than $\mathbf{f}_a$, meaning that the inertial time τ_0 is smaller than τ.

The dynamics of the polymer center of mass, $\mathbf{r}_c = \sum_n \mathbf{r}_n/N$ and $\mathbf{v}_c = \sum_n \mathbf{v}_n/N$, could be simply obtained by summing up Eqs.(2) for all the monomers:

$$\dot{\mathbf{r}}_c = \mathbf{v}_c \tag{4a}$$

$$\dot{\mathbf{v}}_c = -\frac{\mathbf{v}_c}{\tau_0} + \frac{\mathbf{f}_a}{N} + \frac{\sqrt{2D_t}}{\tau_0\sqrt{N}}\,\boldsymbol{\xi}\,, \tag{4b}$$

being $\boldsymbol{\xi}$ a new white noise vector whose uncorrelated components have unit variance and zero average. The center of mass behaves as a free active particle, where the amplitude of the effective bath scales as $1/\sqrt{N}$ and the active force is decreased by a factor N. The linearity of Eq.(4a) and Eq.(4b) allows us to find the joint probability distribution function of the velocity and the active force of the center of mass:

$$p\,(\mathbf{v}_c, \mathbf{f}_a) \propto G(\mathbf{f}_a)\ \exp\left[-\frac{\beta_{\text{eff}}}{2}\,(\mathbf{v}_c - \mathcal{C}\,\mathbf{f}_a)^2\right]. \tag{5}$$

where $G(\mathbf{f}_a)$ is a Gaussian function centered in zero and the coefficients $\beta_{eff}, \mathcal{C}$ both depend on τ, τ_0, D_a and D_t, see Appendix C. This analysis shows that, given an $\mathbf{f}_a$, $\mathbf{v}_c$ assumes a typical average value $\langle \mathbf{v}_c \rangle \propto \mathbf{f}_a$, thus in a time window smaller than τ, the polymer is driven by the active force whose value is extracted by a Gaussian distribution.

The possibility of the active force to drag the polymer can be easily estimated by comparing the rescaled variance of $\mathbf{f}_a$ with the variance of the thermal bath, in Eq.(4b). The active force on the head to be effective needs to overwhelm the thermal agitation of the passive polymer, thus

$$\frac{D_a}{\tau\, N^2} \gg \frac{D_t}{N\,\tau_0^2}\,. \tag{6}$$

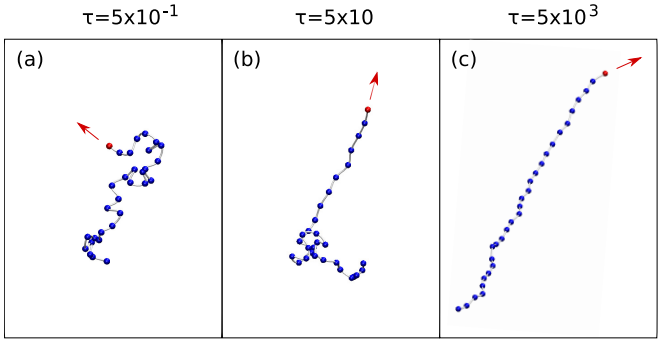


Figure 1. Conformations for three different values of $\tau = 5\times10^{-1}, 5\times10, 5\times10^{4}$, from the left to the right. Each monomer is represented as a sphere centered in $\mathbf{r}_i$ and the grey links among beads are just a guide for the eyes. The head of the polymer is the red monomer, whose active force is drawn as a red vector, while the passive monomers are colored blue. The remaining parameters are $D_a/\tau = 10^2$, $\sigma = 5$, $k = 10$, $T = 1$ and $\tau_0 = 0.1$. Simulations are obtained using a time-step $\sim 10^{-4}$ and each configuration is evolved, at least, for a final time $\sim 10^2\tau$.

This condition follows from the exact formula of the mean square displacement, MSD(t), of the polymer center of mass derived in Appendix C,

$$\mathrm{MSD}(t) = 6\left(\frac{D_t}{N} + \frac{D_a\tau_0^2}{N^2}\right)t + 6\frac{D_a\tau_0^2}{N^2}\tau\left(e^{-t/\tau}-1\right). \quad (7)$$

The linear term dominates in the long-time limit, therefore the active force is able to affect the diffusive dynamics of the center of mass only if $D_a/N \simeq D_t/\tau_0^2$. Instead, for small times, the active force produces a ballistic contribution in the MSD(t) as it can be deduced by expanding the exponential in power of t/τ up to the second order. Even for small times, this term is relevant with respect to the diffusive one if the condition $D_a/\tau/N^2 \gg D_t/N/\tau_0^2$ holds. Throughout the rest of the paper, we assume that both conditions are satisfied: the first increasing the center of mass diffusivity and the second leading to a ballistic time regime.

III. EFFECT OF A LOCAL ACTIVE FORCE ON A FREE POLYMER

Understanding the polymer dynamics beyond Eqs.(4a,4b) requires numerical integration of Eqs. (2). To simulate the dynamics, we employ a stochastic Leapfrog algorithm [62] and focus on some typical observables able to unveil the interplay between the active force and the polymer deformations. Setting a large value of D_a/τ to satisfy the condition (6), we explore a range of small and large τ compared to the relaxation times of the Rouse modes of the passive chain [51]

$$\tau_p = \frac{1}{4k\tau_0\sin^2\left(\frac{p\pi}{2N}\right)}. \quad (8)$$

In Fig.1, we plot three snapshots of the conformations of a polymer with $N = 30$ monomers at different values of τ. Each panel corresponds to $D_a/\tau = 10^2$, at which the polymer center of mass is transported by the active force. In panel (a), when τ is small, the polymer behaves as a passive system, being $\mathbf{f}_a \approx \sqrt{2D_a}\boldsymbol{\eta}$. In this case, indeed, the active force only superimposes an additional Brownian motion to the dynamics of the head. Therefore, the polymer swells a bit, however maintaining the well-known coiled structure of a passive Rouse-chain polymer [51]. Increasing τ, the head starts to pull some of the monomers which protrude from the coil along the direction pointed by the active force, in such a way that an elongated portion of the chain coexists with the remaining coiled portion. In this case, the head has enough time to carry the center of mass and the polymer displays a persistence dynamics in one direction which is slowed down by the "passive" globule. A further increase of τ, panel (c), leads the polymer to be fully elongated in a rod-like conformation which is carried by the active head. The dynamics of the polymer reveals a time-persistence along the random direction pointed by the active force. When the head changes direction (roughly after time $\sim \tau$) the rest of the monomers follows the head, turning with a typical time delay depending on the distance from the head.

To characterize the "global" effect of a local active force on the polymer dynamics, we will monitor the distribution of the end-to-end distance focusing on its moments. Then, we will also explore the "local" effect by quantifying the degree of the stretching produced along the chain by the active head. Finally, we will focus on the velocity of the head, revealing a bump in its variance with the increase of the persistence time.

A. Macroscopic properties of the head-active polymer

To quantify the degree of elongation taken by the polymer, we consider the end-to-end distance

$$\mathcal{R} = |\mathbf{r}_N - \mathbf{r}_1|, \quad (9)$$

and its distribution

$$P(\mathcal{R}) = \langle\delta(\mathcal{R} - |\mathbf{r}_N - \mathbf{r}_1|)\rangle,$$

at different values of τ and for fixed $D_a/\tau = 10^2$. The end-to-end distance, like the gyration radius, is an important observable in polymer physics, providing an estimate of polymer sizes. Its distribution is experimentally accessible by FRET spectroscopy [63, 64], moreover, the

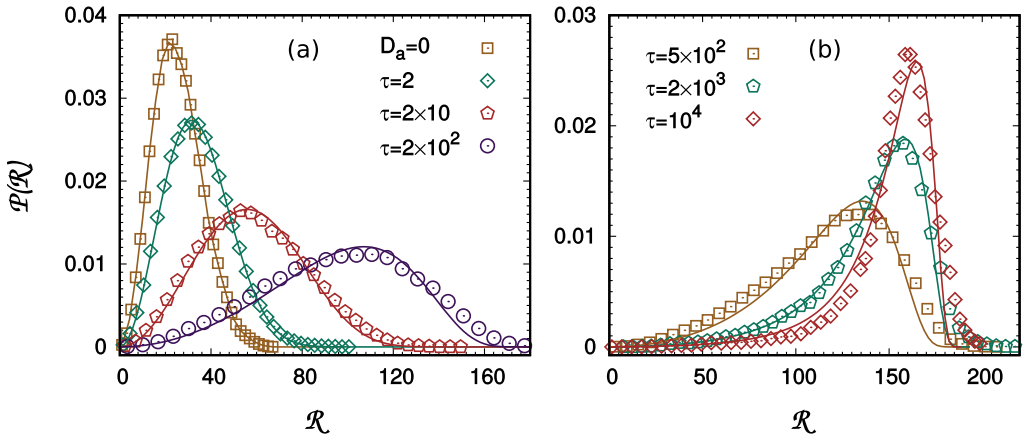


Figure 2. Probability distribution of the end-to-end distance, $\mathcal{P}(\mathcal{R})$, for different values of τ. Points are obtained via numerical simulations while continuous lines from Eq.(10). Data are separated into two panels for presentation reasons: panel (a) refers to small values of τ while panel (b) refers to large values of τ. The remaining parameters are $D_a/\tau = 10^2$, $\sigma = 5$, $k = 10$, $D_t = 0.1$ and $\tau_0 = 0.1$. Simulations are obtained using a time-step $\sim 10^{-4}$ and each configuration is evolved, at least, for a final time $\sim 10^2\tau$.

end-to-end distance is involved in the mechanism of polymer looping and cyclization [65].

Panel (a) of Fig.2 plots $\mathcal{P}(\mathcal{R})$ from numerical simulations at fixed $D_a/\tau = 10^2$ but different values of τ in the interval $0 \div 2 \times 10^2$, corresponding to the range of small persistence. For comparison, we show also the passive case ($D_a = 0$) that, in the limit $N \gg 1$, is simply described by the well known Gaussian-like shape

$$\mathcal{P}(\mathcal{R}) \propto \mathcal{R}^2 \exp\left(-\frac{3}{2}\frac{\mathcal{R}^2}{\langle \mathcal{R}^2\rangle}\right), \tag{10}$$

where $\langle \mathcal{R}^2\rangle$ is the second moment of the distribution. Expression (10) follows as a simple consequence of the central limit theorem. In the low-activity regime, the distribution remains Gaussian-like but with a variance increasing with τ, indicating that, in this regime, the active force is only able to induce a renormalization of the diffusion coefficient. Panel (b) of Fig. 2 reports the $\mathcal{P}(\mathcal{R})$ in the large persistence regime with τ ranging within $5 \times 10^2 \div 10^4$. Starting from $\tau \approx 5 \times 10^2$ strong non-Gaussian effects appear in the shape of $\mathcal{P}(\mathcal{R})$ and Eq.(10) is no longer a reasonable approximation. Specifically, the peak shifts towards larger values of $\mathcal{R}$, the longest tail occurs at small $\mathcal{R}$ and accordingly the skewness of the distribution changes sign. A further increase of τ narrows the distribution and makes it more peaked around $\mathcal{R} = (N-1)\sigma$, corresponding to the end-to-end distance of the entirely elongated chain. Interestingly, the main peak for $\tau > 10^3$ occurs for $\mathcal{R} > (N-1)\sigma$ indicating that the chain is not only elongated but also over-stretched. In this stretched regime, $\mathcal{P}(\mathcal{R})$ weakly depends on τ and its increase produces very small changes in the distribution until a delta-like shape is achieved at very high τ.

The persistence of the active force confers to the chain a certain spatial persistence starting from the active head. This suggests fitting the numerical distributions via the formula

$$\mathcal{P}(\mathcal{R}) \propto \frac{4\pi\mathcal{R}^2}{L^2-\mathcal{R}^2}\exp\left\{-\frac{9L^3}{\ell_p(L^2-\mathcal{R}^2)}\right\}, \tag{11}$$

that was derived for stiff polymers [66]. Where ℓ_p is the effective persistence length of the chain and L is the maximal contour length that includes possible overstretching. The rather good fitting in all the regimes shows that the local active force induces the polymer to behave as if it had a certain degree of stiffness. In the limit of small τ, Eq. (11) recovers the Gaussian-like behavior that is consistent with the globular shape of the polymer (Fig. 2 (a)), while reproduces the shape of $\mathcal{P}(\mathcal{R})$ at large τ (Fig. 2 (b)).

We use the observable $\langle \mathcal{R}^2\rangle$ as an indicator of the crossover from the compact to the elongated structures, visualized in Fig.1. In particular, Fig 3 shows the monotonic increase of $\langle \mathcal{R}^2\rangle$ as a function of τ. The phenomenological theory of stiff polymers, Eq.(11),predicts for $\langle \mathcal{R}^2\rangle$ the expression [66]:

$$\langle \mathcal{R}^2\rangle_{lp} = 2\ell_p L + 2\ell_p^2\left(e^{-L/\ell_p}-1\right). \tag{12}$$

As expected, Eq.(12) fairly agrees with data, as Fig. 3 shows, where l_p is obtained from the numerical fit of relation (11).

To attempt a theoretical prediction on $\langle \mathcal{R}^2\rangle$, going beyond a phenomenological theory, we make the approximation $\sigma \simeq 0$ in the potential (1) transforming the polymer into a Rouse-chain [51]. The expression of $\langle \mathcal{R}^2\rangle$ obtained for the Rouse chain using the normal mode decomposition is (see appendix C),

$$\langle \mathcal{R}^2\rangle = \frac{3D_t}{\tau_0 k}(N-1) + \frac{6D_a\tau_0^2}{N^2}\sum_{(p,q)=1}^{N-1}\frac{c(p)c(q)\,G(p)G(q)}{\gamma_p+\gamma_q}\left[\frac{1}{1+\gamma_p\tau_a}\right], \tag{13}$$

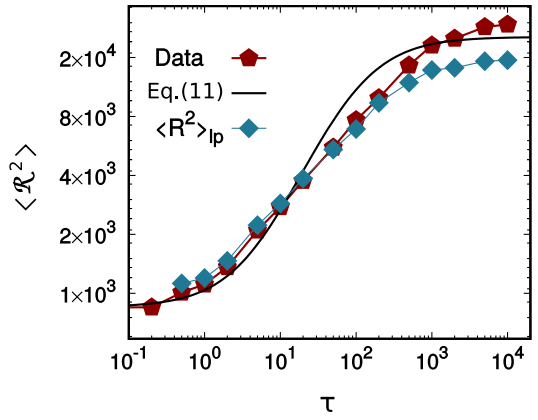


Figure 3. $\langle \mathcal{R}^2 \rangle$ for different values of τ (red pentagons) compared with Eq.(13) (black line) and the prediction, Eq.(12) (light blue diamonds). The remaining parameters are $D_a/\tau = 10^2$, $\sigma = 5$, $k = 10$, $D_t = 0.1$ and $\tau_0 = 0.1$. Simulations are obtained using a time-step $\sim 10^{-4}$ and each configuration is evolved, at least, for a final time $\sim 10^2\tau$.

where $c(p)$ and $G(p)$ are dimensionless coefficients depending only on the index p and on N:

$$G(p) = -4 \sin\left(\frac{p\pi}{2}\right) \sin\left[\frac{p\pi}{2N}(N-1)\right] \tag{14}$$

$$c(p) = \cos\left[\frac{p\pi}{2N}(2N-1)\right]. \tag{15}$$

and $\gamma_p = 1/\tau_p$ (Eq. (8)) has the dimension of an inverse time. Eq.(13) contains two contributions, the first one, entirely due to the thermal agitation of the solvent, is constant and controlled by the ratio $D_t/k\tau_0$. The second one is due to the active force and is controlled by the ratio $D_a\tau_0/k/(1+k\tau\tau_0)$. It is straightforward to see that in the limit $\tau \to 0$ the term $D_a\tau_0 \propto \tau\tau_0$ plays the role of an effective temperature, in agreement with our previous discussion. Moreover, in the equilibrium regime, $\tau = 0$, this term vanishes thus the well-known equilibrium result is recovered. In particular, being the ratio D_a/τ fixed, the small-τ limit implies that the active force gives only a contribution of order $O(\tau)$ to $\langle \mathcal{R}^2 \rangle$. We remark that the active term in Eq. (13) shows a non-trivial dependence on each mode. In Fig. 3, we compare the $\langle \mathcal{R}^2 \rangle$ from simulations (dots) computed at different values of τ with the prediction (13) rescaled by the factor σ^2 since the Rouse chain turns to be more compact than the model (1). Despite the approximation, the prediction fairly agrees with data, both for small and large values of τ.

B. How the active force affects the relaxation times of the modes

The Rouse-chain approximation allows us to study analytically the influence of the local active force on the chain relaxation. Indeed, the time correlation of the generic Rouse-mode, $C_{pp}(t,s)$, can be computed explicitly and reads

$$C_{pp}(t,s) = f_{\rm Th}\frac{e^{-\gamma_p|t-s|}}{2\gamma_p} + \frac{3D_a\tau_0^2}{N^2}c^2(p)\,\frac{\gamma_p\tau e^{-|t-s|/\tau} - e^{-\gamma_p|t-s|}}{\gamma_p[(\gamma_p\tau)^2-1]}\,. \tag{16}$$

The derivation of Eq. (16) is reported in Appendix C. The first term represents the passive contribution of thermal agitation in the absence of any active source of motion. In that case, the p-mode relaxation time is simply $1/\gamma_p$.

The active force gives rise to the second term in Eq. (16), which is the sum of two exponentials. The second exponential survives even in the equilibrium limit $\tau \to 0$ but trivially determines just a renormalization of the auto-correlation amplitude without affecting the correlation time. Instead, in the limit of $\tau \gg 1/\gamma_p$, very interesting consequences emerge as the relaxation is dominated by

$$C_{pp}(t,s) \sim \frac{3\tau_0^2 D_a c^2(p)}{N^2}\frac{\tau e^{-|t-s|/\tau}}{[(\gamma_p\tau)^2-1]}\,, \tag{17}$$

therefore, all the modes decay in the same manner.

In elongated conformations $\tau \gg 1/\gamma_p$ for every p, meaning that τ is the only relevant time in the polymer dynamics. Instead, in the full or partial coiled conformations, we have $1/\gamma_p > \tau$, at least for the lowest p, and the active force is able to affect only the dynamics of the faster modes.

The analysis of these sections suggests that even a local active force on the terminal monomer is able to determine important consequences on the dynamics of the entire polymer, making possible drastic global rearrangements of its conformations.

In the next Section, we investigate the role of the active force at a single monomer level, finding even strong local distortions in the inter-monomer distances.

C. Local effects of the self-propulsion on polymer structures

To understand how the deformation induced by the active force propagates along the chain, for different values of τ, we plot in Fig. 4 (a) the average distance between consecutive monomers, $d_k = \langle |\mathbf{r}_{k+1} - \mathbf{r}_k| \rangle$, as a function of the monomer site k.

In the regime of small active-force persistence, we find $d_k \simeq \sigma$, in analogy with passive polymers in solution; the bond fluctuations are weakly affected by the active force. When τ increases, the average distance between consecutive monomers is no longer constant because there is a transmission of the active-force from the head backward to the tail. Therefore, the bonds near the head, N, result stretched, $d_k \geq \sigma$, and the stretching degree decays to σ for the farther monomers.

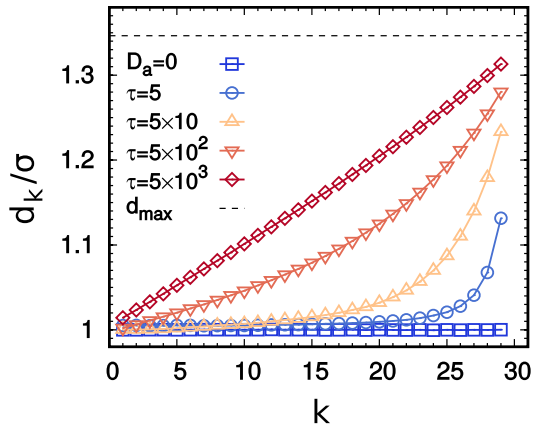


Figure 4. Average distance between neighboring monomers, $r_k/\sigma = \langle|\mathbf{r}_{k+1} - \mathbf{r}_k|\rangle/\sigma$, as a function of the monomer index k for different values of τ, as shown in the legend. The dot black line represents the theoretical prediction for the distance between the head and $N-1$-th monomer, i.e. d_{max}/σ. The remaining parameters are $D_a/\tau = 10^2$, $\sigma = 5$, $k = 10$, $D_t = 0.1$ and $\tau_0 = 0.1$. Simulations are obtained using a time-step $\sim 10^{-4}$ and each configuration is evolved, at least, for a final time $\sim 10^2\tau$.

A further increase of τ is responsible for a larger stretching of the chain till to reach an almost linear profile

$$d_k \simeq \sigma + bk$$

for $\tau \simeq 5 \times 10^3$. Large active forces on the head overstretch the polymer and induce a bond deformation which increases approaching the head. In particular, we note that the average distance between the head and the first passive monomer can be estimated by $d_{\max} = \sigma + \sqrt{3D_a}\tau/k$, thus $b \simeq d_{\max}/(N-1)$. Such a distance can be roughly obtained by replacing f_a with its standard deviation, an assumption which is meaningful as long as τ is large.

In conclusion, we can say that the forcing effects of $\mathbf{f}_a$ propagates backward from the monomer N along the chain establishing a gradient of bond deformation. We remark that this picture is qualitatively reproduced even in the Rouse-chain approximation, as explicitly shown in Appendix C.

It is interesting to observe that the conformation of Fig.1(b) suggests a phenomenology similar to the trumpet formation in polymers pulled by a constant force [67, 68] which is characterized by a scaling law in the tension propagation. The analogy with the trumpet regime is however difficult to establish on a quantitative basis, for two reasons: the moderate size of our chains does not allow this scaling to be verified, our force is not systematic and vanishing on the average.

We, also study the bond-bond spatial correlation along the contour length of the chain, referred to the terminal monomer N, defined as

$$C_N(k) = \langle(\mathbf{r}_N - \mathbf{r}_{N-1}) \cdot (\mathbf{r}_{k+1} - \mathbf{r}_k)\rangle \,. \qquad (18)$$

where the average is computed over stationary chain conformations. Figure 5 (a) plots $C(k)$ vs k, for different values of τ, revealing a monotonic increase moving towards the terminal N. The growth of $C(k)$ is roughly exponential, with a typical length increasing with τ. To confirm the qualitative scenario of stiff polymers, we compare the value of l_p extracted from the fit of $\mathcal{P}(\mathcal{R})$ (Eq. (11)) with the correlation length associated to $C_N(k)$ and extracted from the best exponential fit of each curve in Fig. 5 (a). The plot in Fig. 5 (b) shows the consistency of the two observables, both growing monotonically with τ. This agreement verifies the applicability of the stiff-polymers approach to our active chain.

In Fig. 6 (a), we study the modulus of the velocity probability distribution of the head, $p(|\mathbf{v}_N|)$, showing two typical shapes for a small and a large value of τ. In both cases, the distributions are Gaussian-like:

$$P(|\mathbf{v}_N|) \propto |\mathbf{v}_N|^2 \exp\left(-\frac{|\mathbf{v}_N|^2}{2\langle \mathbf{v}_N^2\rangle}\right), \qquad (19)$$

with different variances, $\langle \mathbf{v}_N^2\rangle$, whose dependence on τ is reported in Fig. 6 (b). The Gaussianity is obvious in the regime of small τ, in particular when the active force can be roughly considered as an additional Brownian noise. In this regime, a first growth of τ determines an enlargement of the variance of the distribution, as shown in panel(b). In particular, the variances are given by $\langle \mathbf{v}_N^2\rangle = 3D_t/\tau_0 + 3D_a\tau_0$. We note also that keeping fixed D_a/τ implies that $D_a \propto \tau$, which explains the initial linear growth with τ in Fig. 6 (b), until a maximal value is reached. The expression $3D_t/\tau_0 + 3D_a\tau_0$ fails for $\tau \geq O(1)$ where the persistence of the motion prevents the interpretation of the active force as another source of diffusion. In this regime, the variance of the distribution decreases again, until a plateau $\langle \mathbf{v}_N^2\rangle = 3D_t/\tau_0$ is reached meaning that the active force does not affect the distribution of $|\mathbf{v}_N|$. This value of the plateau T is not so surprising since $\tau \to \infty$ corresponds to the limit of a constant driving force, which is not expected to influence the fluctuations of $|\mathbf{v}_N|$.

Such a study has revealed a non-monotonous behavior in the variance of the distribution (roughly its effective temperature) which is in agreement with the recent observation [69]: even for an interacting system of spherical particles, the increase of τ induces at first the warming of the system, while a further increase leads to its cooling.

IV. CONCLUSIONS

In this work, we studied the transport of a Rouse-like polymer driven by a local active force localized in the terminal monomer (active head) to characterize the effects of the activity on the chain conformations. Upon increasing the persistence of the self-propulsion, we observed a transition from globular to open conformations, revealing the presence of a regime where random-coil and partially

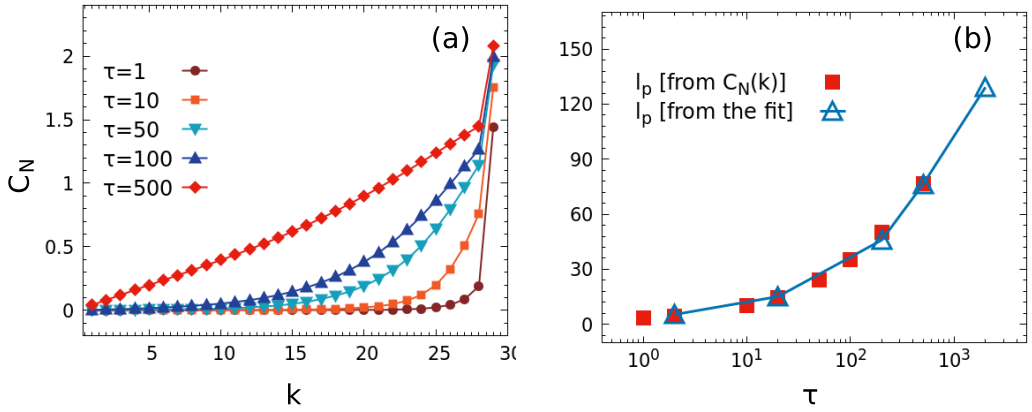


Figure 5. Panel (a): Bond-bond spatial correlation along the contour length of the polymer, $C_N(k)$ (defined by Eq. (18)), as a function of k, shown for different values of τ. Panel (b): l_p as a function of τ, calculated from the fit (blue triangles) of the stiff polymer (Eq. (11)) and the best exponential fit of $C_N(k)$, as explained in the text. The remaining parameters are $D_a/\tau = 10^2$, $\sigma = 5$, $k = 10$, $D_t = 0.1$ and $\tau_0 = 0.1$. Simulations are obtained using a time-step $\sim 10^{-4}$ and each configuration is evolved, at least, for a final time $\sim 10^2\tau$.

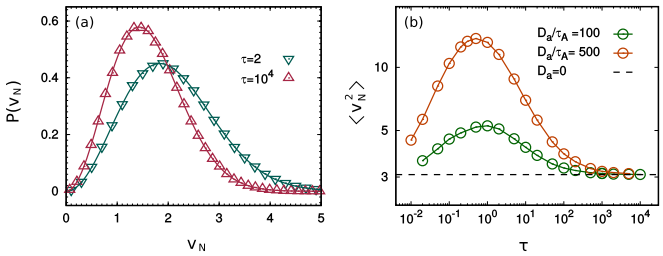


Figure 6. Panel (a): Probability distribution of the head velocity, $P(|\mathbf{v}_N|)$ for two different values of τ at $D_a/\tau = 10^2$. Panel (b): variance of the distribution of $\mathbf{v}_N$ as a function of τ for two different values of D_a/τ, as shown in the legend. The remaining parameters are $\sigma = 5$, $k = 10$, $D_t = 0.1$ and $\tau_0 = 0.1$. Simulations are obtained using a time-step $\sim 10^{-4}$ and each configuration is evolved, at least, for a final time $\sim 10^2\tau$.

elongated conformations coexist. This transition is well-described by the statistics of the end-to-end distance, in particular its distribution and the second moment, whose numerical analysis is supported by theoretical predictions provided by stiff-polymer theory and Rouse-chain calculations. Moreover, we investigated the local properties of the chain focusing both on bond stretching and bond-bond correlation along the contour length, in fair agreement with the phenomenological stiff-polymer theory. We find that the active force acting on the head induces a gradient of bond deformation in regimes of strong persistence, deeply affecting the "microscopic" structural properties of the chain. Our results could be easily generalized to the case of more complex potentials going beyond the simple linearity of the Rouse-chain. Different shapes of the potential lead to the same phenomenology even if the bond stretching could be consistently reduced choosing a stiffer attraction between monomers.

Our study is a contribution towards the comprehension of the complex interplay between shape-deformability and local self-propulsion in extended systems. Generalizing this study to more complex and deformable geometries could represent a very promising point to go beyond the approximation of self-propelled rigid bodies.

ACKNOWLEDGMENT

This research was supported by M.I.U.R., Prin "Coarse-grained description for non-equilibrium systems and transport phenomena" (CO-NEST), Grant n.201798CZLJ.

CONFLICTS OF INTEREST

There are no conflicts of interest to declare.

Appendix A: Strength and persistence time of $\mathbf{f}_a$

In this paper, we employ the AOUP model to reproduce the self-propulsion in three dimensions. This is modeled as a time-dependent force evolving by three independent O.U. processes, i.e. by Eq.(3).

As already explained in the text, τ is the persistence time of the dynamics determining also the correlation time of the auto-correlation of $\mathbf{f}_a$, which reads:

$$\langle \mathbf{f}_a(t) \cdot \mathbf{f}_a(s) \rangle = 3 \frac{D_a}{\tau} \exp\left(-\frac{|t-s|}{\tau} \right).$$

Additionally, since the steady state solution of Eq.(3) (i.e. the marginal probability distribution of $\mathbf{f}_a$) is:

$$p\left(\mathbf{f}_a\right) \propto \exp\left(-\frac{D_a}{\tau} \frac{\left|\mathbf{f}_a\right|^2}{6} \right),$$

it is straightforward to conclude that the square root variance of the active force, which is proportional to D_a/τ, determines the strength of the self-propulsion force, being $\langle |\mathbf{f}_a| \rangle = \sqrt{D_a/\tau}$.

Appendix B: Velocity distribution of the center of mass

The dynamics of the center of mass, Eqs. (4), and of the self-propulsion, Eqs. (4), can be analyzed by deriving the associated Fokker-Planck equation [70] governing the evolution of the probability distribution $f(\mathbf{x}_c, \mathbf{v}_c, \mathbf{f}_a, t)$,

$$\partial_t f = \frac{\nabla_{\mathbf{v}_c}}{\tau_0} \cdot \left(\mathbf{v}_c f - \frac{\tau_0}{N} \mathbf{f}_a f \right) + \frac{D_t}{N \tau_0^2} \nabla^2_{\mathbf{v}_c} f - \mathbf{v}_c \cdot \nabla_{\mathbf{x}_c} f + \nabla_{\mathbf{f}_a} \cdot \left(\frac{\mathbf{f}_a}{\tau} f \right) + \frac{D_a}{\tau^2} \nabla^2_{\mathbf{f}_a} f \tag{B1}$$

where ∇ and ∇^2 indicate the gradient and the Laplacian operator, with respect to the variables in the subscript. These equation is diffusive in space, but admits a steady-state distribution, $p(\mathbf{v}_c, \mathbf{f}_a)$, in velocity and self-propulsion. The linearity of the process implies that $p(\mathbf{v}_c, \mathbf{f}_a)$ is a multivariate Gaussian

$$p(\mathbf{v}_c, \mathbf{f}_a) \propto G(\mathbf{f}_a) \ \exp\left[-\frac{\beta_{\text{eff}}}{2} \left(\mathbf{v}_c - \frac{\mathcal{C}}{N} \mathbf{f}_a \right)^2 \right],$$

$$G(\mathbf{f}_a) \propto \exp\left[-\left(1 + \frac{\Gamma^4}{(1+\Delta)^2} \frac{\tau}{\tau_0} \frac{1}{\frac{1}{\Gamma} + \Delta + \frac{\tau}{\tau_0} \frac{\Gamma^3}{(1+\Delta)^2}} \right) \frac{\tau}{D_a} \frac{\mathbf{f}_a^2}{2\,N} \right],$$

where the coefficients reads:

$$\beta_{eff} = \frac{1}{\tau_0 D_a} \left(\frac{1}{\frac{1}{\Gamma} + \Delta} + \frac{\tau}{\tau_0} \frac{\Gamma^3}{(1+\Delta)^2} \right),$$

$$\mathcal{C} = \frac{\Gamma^2}{1+\Delta} \frac{1}{\frac{1}{\frac{1}{\Gamma} + \Delta} + \frac{\tau}{\tau_0} \frac{\Gamma^3}{(1+\Delta)^2}},$$

being $\Gamma = 1 + \tau/\tau_0$ and $\Delta = D_t N/(\tau_0^2 D_a)$.

Appendix C: Rouse-mode analysis of correlations

Rouse model, whose potential energy is Eq.(1) with $\sigma = 0$, can be analytically solved by a decompositions in Rouse-modes

$$\mathbf{r}_n(t) = \mathbf{X}_0(t) + 2 \sum_{p=1}^{N-1} \mathbf{X}_p(t) \cos\left[\frac{p\pi}{N} \left(n - \frac{1}{2} \right) \right] \tag{C1}$$

where each mode, defined as

$$\mathbf{X}_p(t) = \frac{1}{N} \sum_{n=1}^{N} \mathbf{r}_n(t) \cos\left[\frac{p\pi}{N} \left(n - \frac{1}{2} \right) \right],$$

is independent of the others and evolves, in the stationary regime, according to

$$\mathbf{X}_p(t) = \tau_0 e^{-\gamma_p t} \int_{-\infty}^{t} ds\; e^{\gamma_p s} [\mathbf{F}_p(s) + \mathbf{A}_p(s)]\,, \tag{C2}$$

with $\mathbf{F}_p$ and $\mathbf{A}_p$ the mode components of the Brownian and active force, respectively. Instead, γ_p is given by

$$\gamma_p = 4\,k\,\tau_0 \sin^2\left(\frac{p\pi}{2N}\right),$$

being k the stiffness of the chain and τ_0 the relaxation time of the solvent.

A central quantity of our approach is the stationary time-correlation between the modes for $p > 0$ and $q > 0$, i.e.

$$C_{pq}(t-s) = \langle \mathbf{X}_p(t)\mathbf{X}_q(s)\rangle\,,$$

that can be evaluated by using Eq.(C2),

$$\langle \mathbf{X}_p(t)\cdot\mathbf{X}_q(s)\rangle = \tau_0^2 e^{-(\gamma_p t+\gamma_q)s} \int_{-\infty}^{t} du \int_{-\infty}^{s} dv e^{\gamma_p u+\gamma_q v'} \Big[\langle \mathbf{F}_p(u)\cdot\mathbf{F}_q(v)\rangle + \langle \mathbf{A}_p(u)\cdot\mathbf{A}_q(v)\rangle\Big]\,.$$

The correlations of the Fourier components of the thermal and active noises can be easily derived from the direct correlation of such noises considered in Eqs.(2),

$$\langle \mathbf{F}_p(s)\cdot\mathbf{F}_q(s')\rangle = \frac{3D_t}{N\tau_0^2}\Big[\delta(p+q)+\delta(p-q)\Big]\delta(s'-s) \tag{C3}$$

$$\langle \mathbf{A}_p(s)\cdot\mathbf{A}_q(s')\rangle = \frac{3D_a}{N^2\tau} c(p)c(q)\exp(-|s'-s|/\tau)\,. \tag{C4}$$

Thus $C_{pq}(t-s)$ is expressed by the sum of two terms

$$C_{pq}(t-s) = f_{\rm Th}\delta_{p,q}\frac{e^{-\gamma_p|t-s|}}{2\gamma_p} + f_{\rm Act}c(p)c(q)S_{pq}(t-s);$$

where

$$c(p) = \cos\left[\frac{p\pi}{2N}(2N-1)\right] = (-1)^p\cos\left[\frac{p\pi}{2N}\right].$$

and the two constants are defined as

$$f_{\rm Th} = \frac{3D_t}{N} \quad , \quad f_{\rm Act} = \frac{3D_a\tau_0^2}{N^2}\,.$$

The last term in $C_{pq}(t-s)$ refers to the active force and contains the integral

$$S_{pq}(t-s) = \frac{1}{\tau}\int_{-\infty}^{t} du \int_{-\infty}^{u} du e^{\gamma_p(u-t)+\gamma_q(v-s)} e^{-|u-v|/\tau}$$

which can be solved providing the result

$$S_{pq}(t-s) = \begin{cases} \dfrac{\tau e^{-|t-s|/\tau}}{(\gamma_q\tau+1)(\gamma_p\tau-1)} - \dfrac{2e^{-\gamma_p|t-s|}}{(\gamma_p+\gamma_q)(\gamma_p^2\tau^2-1)} & t > s \\[2ex] \dfrac{\tau e^{-|t-s|/\tau}}{(\gamma_p\tau+1)(\gamma_q\tau-1)} - \dfrac{2e^{-\gamma_q|t-s|}}{(\gamma_p+\gamma_q)(\gamma_q^2\tau^2-1)} & t < s \end{cases}. \tag{C5}$$

When $p = q > 0$, we are left with the mode-mode autocorrelation which simplifies to

$$C_{pp}(t,s) = f_{\rm Th}\frac{e^{-\gamma_p|t-s|}}{2\gamma_p} + f_{\rm Act}c^2(p)\,\frac{\gamma_p\tau e^{-|t-s|/\tau} - e^{-\gamma_p|t-s|}}{\gamma_p[(\gamma_p\tau)^2-1]}\,.$$

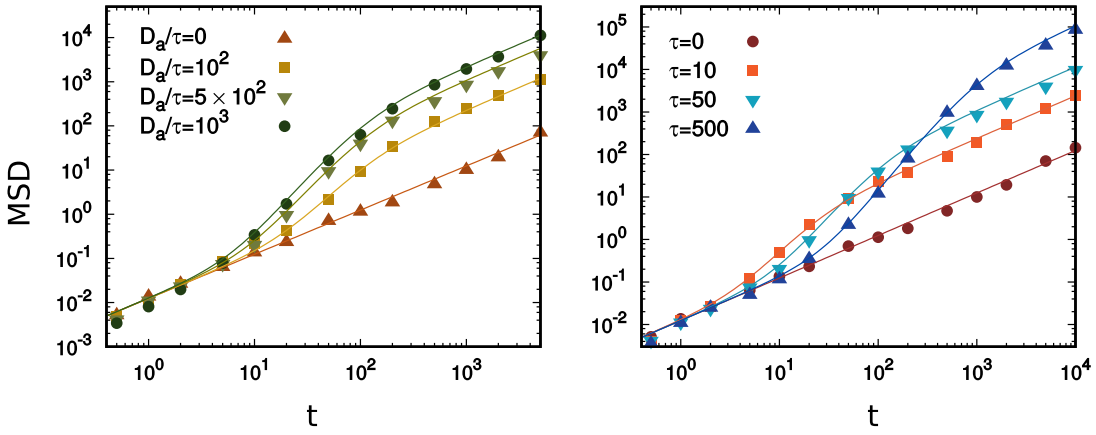


Figure 7. $MSD(t)$ for different values of the active force parameters. In panel (a) we adopt the protocol i), namely varying D_a/τ at fixed $\tau = 50$, while we employ the protocol ii) in panel (b), i.e. varying τ keeping fixed $D_a/\tau = 500$. The remaining parameters are $\sigma = 5$, $k = 10$, $D_t = 0.1$ and $\tau_0 = 0.1$. Simulations are obtained using a time-step $\sim 10^{-4}$ and each configuration is evolved, at least, for a final time $\sim 10^2\tau$.

In the following, we will need the correlation at the same time, $t = s$, a quantity that, in the stationary regime, becomes independent of time and reads

$$C_{pq}(0) = f_{\rm Th}\frac{\delta_{p,q}}{2\gamma_p} + f_{\rm Act}c(p)c(q)\; S_{pq}(0), \tag{C6}$$

with the obvious notation [see. Eq.(C5)]

$$S_{pq}(0) = \frac{1}{\gamma_p+\gamma_q}\left[\frac{1}{\gamma_p\tau+1} + \frac{1}{\gamma_q\tau+1}\right].$$

1. Center of mass behaviour

The center of mass, corresponding to the mode $p = 0$, and given by

$$\mathbf{X}_0(t) = \frac{1}{N}\sum_{n=1}^{N}\mathbf{r}_n(t)$$

evolves in time from the initial condition $\mathbf{X}_0(0)$ as

$$\mathbf{X}_0(t) = \mathbf{X}_0(0) + \tau_0\int_0^t ds\,\left[\mathbf{F}_p(s) + \mathbf{A}_p(s)\right]. \tag{C7}$$

Therefore, its mean square displacement (MSD) will behave as

$$\langle[\mathbf{X}_0(t) - \mathbf{X}_0(0)]^2\rangle = \tau_0^2\int_0^t ds\int_0^t ds'\,\left[\langle\mathbf{F}_0(s)\cdot\mathbf{F}_0(s')\rangle + \langle\mathbf{A}_0(s)\cdot\mathbf{A}_0(s')\rangle\right].$$

The two-time correlations involved are given by Eqs.(C3,C4) taken for $p = q = 0$

$$\langle\mathbf{F}_0(s)\cdot\mathbf{F}_0(s')\rangle = \frac{6\,D_t}{N\tau_0^2}\delta(s-s')$$
$$\langle\mathbf{A}_0(s)\cdot\mathbf{A}_0(s')\rangle = \frac{3D_a}{N^2\tau}\exp\left(-\frac{|s-s'|}{\tau}\right),$$

Thus, Eq.(**??**) turns into

$$\mathrm{MSD}(t) = \frac{6D_t}{N}t + \tau_0^2\frac{3D_a}{N^2\tau}\int_0^t ds\int_0^t ds'\; e^{-|s-s'|/\tau}.$$

In particular, performing the integrals, we get the time-dependent expression for the MSD:

$$\mathrm{MSD}(t) = 6\left(\frac{D_t}{N} + \frac{D_a\tau_0^2}{N^2}\right) t + 6\frac{D_a\tau_0^2}{N^2}\tau\left(e^{-t/\tau} - 1\right).$$

Expanding in power of t/τ we can estimate the relevance of the active force for small t. In particular, we get

$$\mathrm{MSD}(t) \approx 6\frac{D_t}{N}t + 3\frac{D_a\tau_0^2}{N^2}\frac{t^2}{\tau}.$$

Comparing the amplitudes of the two terms, we have a necessary condition to establish the relevance of the active force to the center of mass motion of the polymer even at early stages.

The exact expression for the $MSD(t)$, Eq.(7), is supported by a numerical comparison via two protocols: i) constant τ varying the ratio D_a/τ, ii) varying τ keeping fixed D_a/τ. In both cases, the active force increases monotonically the diffusivity and the agreement between the two sets of data is fairly good as revealed by Fig.7 (a) and (b), respectively.

2. End-to-End Distance

In the active Rouse-model approximation, we can compute analytically the end-to-end distance, $\boldsymbol{\mathcal{R}}(t) = \mathbf{r}_N - \mathbf{r}_1$, of the Rouse Polymer, which reads:

$$\boldsymbol{\mathcal{R}}(t) = 2\sum_{p=1}^{N-1}\mathbf{X}_p(t)\left(\cos\left[\frac{p\pi}{2N}(2N-1)\right] - \cos\left[\frac{p\pi}{2N}\right]\right).$$

This equation can be written formally as the series

$$\boldsymbol{\mathcal{R}}(t) = \sum_{p=1}^{N-1} G(p)\mathbf{X}_p(t),$$

where

$$G(p) = [(-1)^p - 1]\cos\left(\frac{p\pi}{2N}\right).$$

Therefore, its variance can be expressed in terms of the stationary correlation of the modes at the same time

$$\langle\mathcal{R}^2(t)\rangle = \sum_{(p,q)=1}^{N-1} G(p)G(q)\,\langle\mathbf{X}_p(t)\cdot\mathbf{X}_q(t)\rangle, \tag{C8}$$

where $\langle\mathbf{X}_p(t)\cdot\mathbf{X}_q(t)\rangle$ is nothing but Eq.(C6). Thus we obtain the mean square end-to-end distance, i.e. the second moment of $\mathcal{P}(\mathcal{R})$:

$$\langle\mathcal{R}^2(\infty)\rangle = f_{\mathrm{Th}}\sum_{p=1}^{N-1}\frac{G^2(p)}{2\gamma_p} + f_{\mathrm{Act}}\sum_{(p,q)=1}^{N-1}\frac{c(p)c(q)\,G(p)G(q)}{\gamma_p+\gamma_q}\left[\frac{1}{1+\gamma_p\tau} + \frac{1}{1+\gamma_q\tau}\right].$$

The symmetry in p, q implies that the expression can be recast into

$$\langle\mathcal{R}^2\rangle = f_{\mathrm{Th}}\sum_{p=1}^{N-1}\frac{G^2(p)}{2\gamma_p} + 2f_{\mathrm{Act}}\sum_{(p,q)=1}^{N-1}\frac{c(p)c(q)\,G(p)G(q)}{\gamma_p+\gamma_q}\left[\frac{1}{1+\gamma_p\tau_a}\right].$$

It can be shown that for a Rouse-Chain the following sum-rules hold true

$$\sum_{p=1}^{N-1}\frac{G^2(p)}{2\gamma_p} = \frac{N(N-1)}{\tau_0 k}$$

$$\sum_{p=1}^{N-1}G^2(p) = 4N.$$

Thus, the final expression for the mean square end-to-end distance reads

$$\langle \mathcal{R}^2 \rangle = \frac{3D_t}{k}(N-1) + \frac{6D_a\tau_0^2}{N^2}\sum_{(p,q)=1}^{N-1} \frac{c(p)c(q)\,G(p)G(q)}{\gamma_p+\gamma_q}\left[\frac{1}{1+\gamma_p\tau}\right],$$

which coincides with the result of the main text.

3. Fluctuation of the bond deformation

With the same strategy applied to derive the End-to-End distance, we can compute the fluctuation of the bond deformation, $\delta\mathbf{r}_n = \mathbf{r}_{n+1} - \mathbf{r}_n$, induced by the active force along the Rouse chain, i.e.

$$\delta\mathbf{r}_n = 2\sum_{p=1}^{N-1}\mathbf{X}_p(t)\cos\left[\frac{p\pi}{N}\left(n+\frac{1}{2}\right)\right] - \cos\left[\frac{p\pi}{N}\left(n-\frac{1}{2}\right)\right].$$

In a more explicit form, it can be expressed as

$$\delta\mathbf{r}_n = -4\sum_{p=1}^{N-1}\mathbf{X}_p(t)\sin\left(\frac{p\pi}{2N}\right)\sin\left(\frac{p\pi}{N}n\right).$$

For the sake of shortness, it is convenient to set $G_n(p) = 4\sin(p\pi/2N)\sin(q\pi n/N)$. Squaring and averaging, we obtain

$$\langle(\delta\mathbf{r}_n)^2\rangle = \sum_{pq}\langle\mathbf{X}_p(t)\mathbf{X}_q(t)\rangle G_n(p)G_n(q).$$

Since the bond fluctuation depends on the correlation at the same time, it can be rewritten in terms of Eq.(C6)

$$\langle(\delta\mathbf{r}_n)^2\rangle = f_{\rm Th}\sum_{p=1}^{N-1}\frac{G_n(p)}{2\gamma_p} + f_{\rm Act}\sum_{(p,q)=1}^{N-1} c(p)c(q)S_{pq}(0)G_n(p)G_n(q).$$

After some simple algebraic manipulations, and using the definition of $c(p)$, $G_n(p)$ and γ_p, we obtain the long expression

$$\langle(\delta\mathbf{r}_n)^2\rangle = \frac{3D_t}{k\tau_0} + 4f_{\rm Act}\sum_{(p,q)=1}^{N-1}(-1)^{p+q}S_{pq}(0)\sin\left(\frac{p\pi}{N}\right)\sin\left(\frac{q\pi}{N}\right)\sin\left(\frac{p\pi}{N}n\right)\sin\left(\frac{q\pi}{N}n\right).$$

Finally, we can estimate $\langle|\mathbf{r}_{n+1}-\mathbf{r}_n|\rangle \approx \sqrt{\langle(\delta\mathbf{r}_n)^2\rangle}$. As shown in Fig.8, this expression reproduces qualitatively the behavior reported in Fig.4 despite the employment of the Rouse-approximation. We remark that Eq. (C 3) decays to a value smaller than σ for monomers far from the head at variance with Fig.4. This is not surprising since, in the Rouse approximation, σ does not play any role and, thus, even the passive polymer assumes a more compact configuration.

[1] C. Bechinger, R. Di Leonardo, H. Löwen, C. Reichhardt, G. Volpe and G. Volpe, *Reviews of Modern Physics*, 2016, **88**, 045006.

[2] J. Elgeti, R. G. Winkler and G. Gompper, *Reports on progress in physics*, 2015, **78**, 056601.

[3] A. J. Ridley, M. A. Schwartz, K. Burridge, R. A. Firtel, M. H. Ginsberg, G. Borisy, J. T. Parsons and A. R. Horwitz, *Science*, 2003, **302**, 1704–1709.

[4] S. Ganguly, L. S. Williams, I. M. Palacios and R. E. Goldstein, *Proceedings of the National Academy of Sciences*, 2012, **109**, 15109–15114.

[5] C. A. Weber, R. Suzuki, V. Schaller, I. S. Aranson, A. R. Bausch and E. Frey, *Proceedings of the National Academy of Sciences*, 2015, **112**, 10703–10707.

[6] H. Löwen, *EPL (Europhysics Letters)*, 2018, **121**, 58001.

[7] B. Biswas, R. K. Manna, A. Laskar, P. S. Kumar, R. Adhikari and G. Kumaraswamy, *ACS nano*, 2017, **11**, 10025–10031.

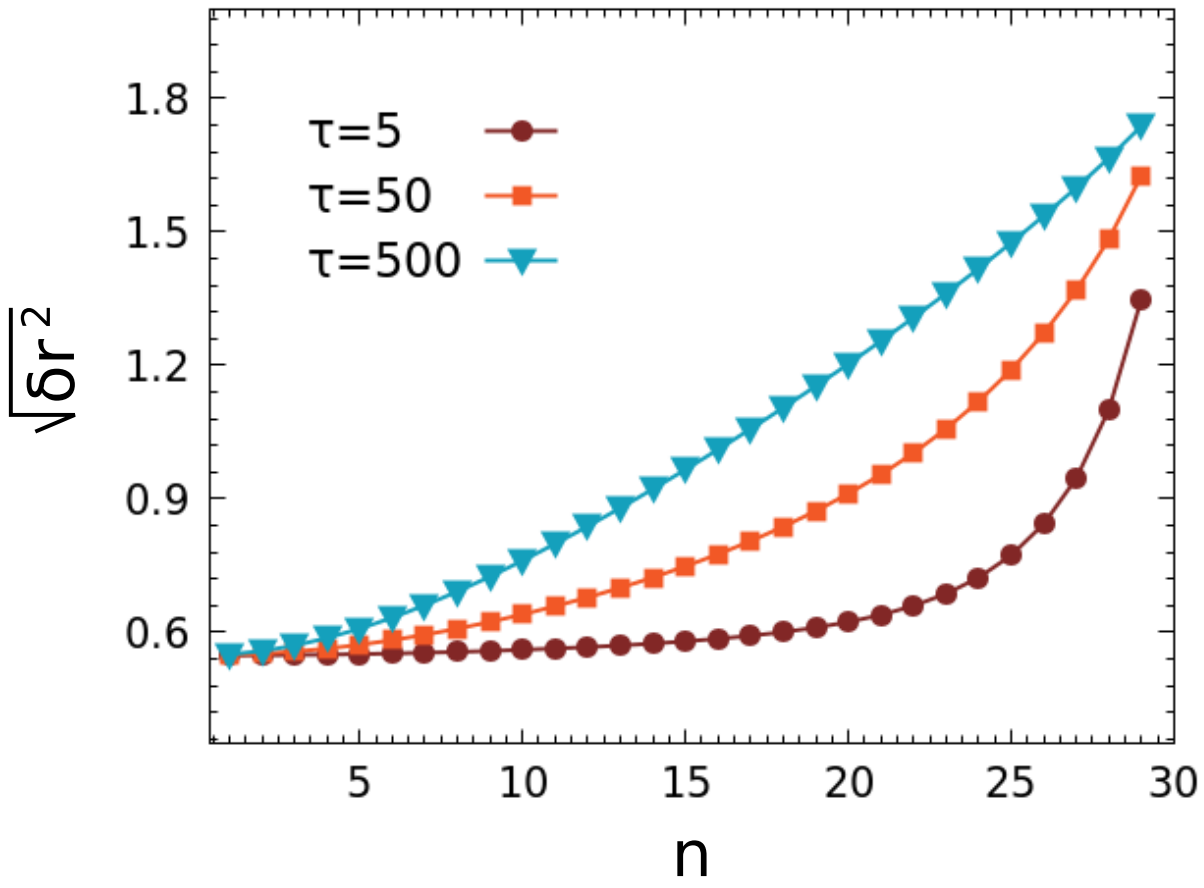


Figure 8. Eq. (C 3) as a function of n for three different values of τ as shown in the legend. The remaining parameters are $D_a/\tau = 10^2$, $\sigma = 5$, $k = 10$, $D_t = 0.1$ and $\tau_0 = 0.1$. Simulations are obtained using a time-step $\sim 10^{-4}$ and each configuration is evolved, at least, for a final time $\sim 10^2\tau$.

[8] R. Di Leonardo, *Nature materials*, 2016, **15**, 1057.
[9] J. Yan, M. Han, J. Zhang, C. Xu, E. Luijten and S. Granick, *Nature materials*, 2016, **15**, 1095.
[10] D. Nishiguchi, J. Iwasawa, H.-R. Jiang and M. Sano, *New Journal of Physics*, 2018, **20**, 015002.
[11] F. C. MacKintosh and P. A. Janmey, *Curr. Opin. Solid St. M.*, 1997, **2**, 350–357.
[12] T. Eisenstecken, G. Gompper and R. G. Winkler, *Polymers*, 2016, **8**, 304.
[13] A. Kaiser, S. Babel, B. ten Hagen, C. von Ferber and H. Löwen, *J. Chem. Phys.*, 2015, **142**, 124905.
[14] J. Shin, A. G. Cherstvy, W. K. Kim and R. Metzler, *New J. Phys.*, 2015, **17**, 113008.
[15] S. Chaki and R. Chakrabarti, *J. Chem. Phys.*, 2019, **150**, 094902.
[16] A. Kaiser and H. Löwen, *J. Chem. Phys.*, 2014, **141**, 044903.
[17] N. Nikola, A. P. Solon, Y. Kafri, M. Kardar, J. Tailleur and R. Voituriez, *Phys. Rev. Lett.*, 2016, **117**, 098001.
[18] J. Harder, C. Valeriani and A. Cacciuto, *Phys. Rev. E*, 2014, **90**, 062312.
[19] N. Samanta and R. Chakrabarti, *Journal of Physics A: Mathematical and Theoretical*, 2016, **49**, 195601.
[20] A. Ghosh and N. S. Gov, *Biophys. J.*, 2014, **107**, 1065–1073.
[21] R. E. Isele-Holder, J. Elgeti and G. Gompper, *Soft matter*, 2015, **11**, 7181–7190.
[22] R. E. Isele-Holder, J. Jäger, G. Saggiorato, J. Elgeti and G. Gompper, *Soft Matter*, 2016, **12**, 8495–8505.
[23] A. Laskar and R. Adhikari, *New J. Phys.*, 2017, **19**, 033021.
[24] R. Chelakkot, R. G. Winkler and G. Gompper, *Phys. Rev. Lett.*, 2012, **109**, 178101.
[25] X. Liu, H. Jiang and Z. Hou, *The Journal of Chemical Physics*, 2019, **151**, 174904.
[26] O. C. Rodriguez, A. W. Schaefer, C. A. Mandato, P. Forscher, W. M. Bement and C. M. Waterman-Storer, *Nature Cell Biol.*, 2003, **5**, 599.
[27] S. J. DeCamp, G. S. Redner, A. Baskaran, M. F. Hagan and Z. Dogic, *Nature Materials*, 2015, **14**, 1110.
[28] Y. Sumino, K. H. Nagai, Y. Shitaka, D. Tanaka, K. Yoshikawa, H. Chaté and K. Oiwa, *Nature*, 2012, **483**, 448.
[29] V. Schaller, C. Weber, E. Frey and A. R. Bausch, *Soft Matter*, 2011, **7**, 3213–3218.
[30] V. Schaller and A. R. Bausch, *Proc. Natl. Acad. Sci.*

USA, 2013, **110**, 4488–4493.
[31] K. Prathyusha, S. Henkes and R. Sknepnek, *Physical Review E*, 2018, **97**, 022606.
[32] G. Vliegenthart, A. Ravichandran, M. Ripoll, T. Auth and G. Gompper, *arXiv preprint arXiv:1902.07904*, 2019.
[33] H. Jiang and Z. Hou, *Soft Matter*, 2014, **10**, 1012–1017.
[34] D. Sarkar and S. Thakur, *Phys. Rev. E*, 2016, **93**, 032508.
[35] S. K. Anand and S. P. Singh, *Physical Review E*, 2018, **98**, 042501.
[36] R. Chelakkot, A. Gopinath, L. Mahadevan and M. F. Hagan, *J. Royal Soc. Interface*, 2014, **11**, 20130884.
[37] S. K. Anand, R. Chelakkot and S. P. Singh, *Soft matter*, 2019, **15**, 7926–7933.
[38] V. Bianco, E. Locatelli and P. Malgaretti, *Physical Review Letters*, 2018, **121**, 217802.
[39] Ö. Duman, R. E. Isele-Holder, J. Elgeti and G. Gompper, *Soft matter*, 2018, **14**, 4483–4494.
[40] J. Smrek and K. Kremer, *Physical Review Letters*, 2017, **118**, 098002.
[41] J. Smrek and K. Kremer, *Entropy*, 2018, **20**, 520.
[42] M. Foglino, E. Locatelli, C. Brackley, D. Michieletto, C. Likos and D. Marenduzzo, *Soft matter*, 2019, **15**, 5995–6005.
[43] Y.-G. Tao and R. Kapral, *ChemPhysChem*, 2009, **10**, 770–773.
[44] D. Sarkar, A. Brahmanandan and S. Thakur, Macromolecular Symposia, 2015, pp. 133–140.
[45] U. M. B. Marconi, N. Gnan, M. Paoluzzi, C. Maggi and R. Di Leonardo, *Scientific Reports*, 2016, **6**, 23297.
[46] É. Fodor and M. C. Marchetti, *Physica A: Statistical Mechanics and its Applications*, 2018, **504**, 106–120.
[47] L. Caprini, U. M. B. Marconi and A. Vulpiani, *Journal of Statistical Mechanics: Theory and Experiment*, 2018, **2018**, 033203.
[48] R. Wittmann, F. Smallenburg and J. M. Brader, *The Journal of chemical physics*, 2019, **150**, 174908.
[49] L. Berthier, E. Flenner and G. Szamel, *The Journal of chemical physics*, 2019, **150**, 200901.
[50] L. Caprini, U. Marini Bettolo Marconi, A. Puglisi and A. Vulpiani, *J. Chemi. Phys.*, 2019, **150**, 024902.
[51] P. E. Rouse, *J. Chem. Phys.*, 1953, **21**, 1272.
[52] Y. Fily and M. C. Marchetti, *Physical Review Letters*, 2012, **108**, 235702.
[53] M. Marchetti, J. Joanny, S. Ramaswamy, T. Liverpool, J. Prost, M. Rao and R. A. Simha, *Reviews of Modern Physics*, 2013, **85**, 1143–1189.
[54] U. Basu, S. N. Majumdar, A. Rosso and G. Schehr, *Physical Review E*, 2019, **100**, 062116.
[55] J. T. Siebert, J. Letz, T. Speck and P. Virnau, *Soft Matter*, 2017, **13**, 1020–1026.
[56] É. Fodor, C. Nardini, M. E. Cates, J. Tailleur, P. Visco and F. van Wijland, *Physical Review Letters*, 2016, **117**, 038103.
[57] L. Caprini and U. M. B. Marconi, *Soft matter*, 2018, **14**, 9044–9054.
[58] L. Caprini, U. M. B. Marconi, A. Puglisi and A. Vulpiani, *Journal of Statistical Mechanics: Theory and Experiment*, 2019, **2019**, 053203.
[59] E. Woillez, Y. Zhao, Y. Kafri, V. Lecomte and J. Tailleur, *Phys. Rev. Lett.*, 2019, **122**, 258001.
[60] S. Das, G. Gompper and R. G. Winkler, *New Journal of Physics*, 2018, **20**, 015001.
[61] L. Caprini, E. Hernàndez-Garcìa, C. Lòpez and U. M. B. Marconi, *Scientific Reports*, 2019, **9**, 16687.
[62] K. Burrage, I. Lenane and G. Lythe, *SIAM J Sci Comput.*, 2007, **29**, 245–264.
[63] A. Soranno, R. Longhi, T. Bellini and M. Buscaglia, *Biophys. J.*, 2009, **96**, 1515–1528.
[64] E. P. O'Brien, G. Morrison, B. R. Brooks and D. Thirumalai, *J Chem. Phys.*, 2009, **130**, 124903.
[65] M. A. Winnik, *Acc. Chem. Res.*, 1985, **18**, 73–79.
[66] J. Bhattacharjee, D. Thirumalai and J. Bryngelson, *arXiv preprint cond-mat/9709345*, 1997.
[67] P. Rowghanian and A. Y. Grosberg, *The Journal of Physical Chemistry B*, 2011, **115**, 14127–14135.
[68] P. Rowghanian and A. Y. Grosberg, *Physical Review E*, 2012, **86**, 011803.
[69] L. Caprini, U. M. B. Marconi and A. Puglisi, *Scientific Reports*, 2019, **9**, 1386.
[70] C. Gardiner, *Handbook of Stochastic Methods for Physics, Chemistry and Natural Sciences*, Springer, 3rd edn., 1985.